Final Draft
of the original manuscript

Safarik, I.; Prochazkova, J.; Schroer, M.; Garamus, V.; Kopcansky, P.; Timko, M.; Rajnak, M.; Karpets, M.; Ivankov, O.; Avdeev, M.; Petrenko, V.; Bulavin, L.; Pospiskova, K.:

Cotton Textile/Iron Oxide Nanozyme Composites with Peroxidase-like Activity: Preparation, Characterization, and Application.

Cotton textile/iron oxide nanozyme composites with peroxidase-like activity: Preparation, characterization and application

Ivo Safarik [1,2,3,*], Jitka Prochazkova [1], Martin A. Schroer [4,*], Vasil M. Garamus [5], Peter Kopcansky [3,*], Milan Timko [3], Michal Rajnak [3,6], Maksym Karpets [3,6], Oleksandr I. Ivankov [7], Mikhail V. Avdeev [7], Viktor I. Petrenko [8,9,*], Leonid Bulavin [10], Kristyna Pospiskova [1,2]

[1] Department of Nanobiotechnology, Biology Centre, ISB, CAS, Na Sadkach 7, 370 05 Ceske Budejovice, Czech Republic

[2] Regional Centre of Advanced Technologies and Materials, Czech Advanced Technology and Research Institute, Palacky University, Slechtitelu 27, 783 71 Olomouc, Czech Republic

[3] Department of Magnetism, Institute of Experimental Physics, SAS, Watsonova 47, 040 01 Kosice, Slovakia

[4] European Molecular Biology Laboratory (EMBL), Hamburg outstation c/o DESY, Notkestr. 85, 22607, Hamburg, Germany

[5] Helmholtz-Zentrum Geesthacht, Centre for Materials and Coastal Research, Max-Planck-Str. 1, Geesthacht 21502, Germany

6 Faculty of Electrical Engineering and Informatics, Technical University of Košice, Letná 9, 04200 Košice, Slovakia

7 Joint Institute for Nuclear Research, Dubna, Moscow region, Russia

8 BCMaterials, Basque Center for Materials, Applications and Nanostructures, Leioa, Spain

9 IKERBASQUE, Basque Foundation for Science, Bilbao, Spain

10 Taras Shevchenko National University of Kyiv, 64/13, Volodymyrs'ka Str., Kyiv 01601, Ukraine

ABSTRACT: At present both native and immobilized nanoparticles are of great importance in many areas of science and technology. In this paper we have studied magnetic iron oxide nanoparticles and their aggregates bound on woven cotton textiles employing two simple modification procedures. One modification was based on textile treatment with perchloric acid stabilized magnetic fluid diluted with methanol followed by drying. The second procedure was based on the microwave assisted conversion of ferrous sulfate at high pH followed by drying. The structure and functional properties of these modified textiles were analyzed in detail. Scanning electron microscopy of native and modified textile clearly showed the presence of iron oxide nanoparticles on the surface of modified cotton fibers. All the modified textiles exhibited light to dark brown color depending on the amount of bound iron oxide particles. Magnetic measurements

showed that the values of saturation magnetization are reflecting the quantity of magnetic nanoparticles present in the modified textiles. Small-angle X-ray and neutron scattering measurements were conducted for the detailed structural characterization at the nanoscale of both the native and magnetically modified textiles and different structural organization of nanoparticles in two kind of textile samples were concluded. The textile-bound iron oxide particles exhibited peroxidase-like activity when measured with N,N-diethyl-p-phenylenediamine sulfate salt substrate; this nanozyme activity enabled rapid decolorization of crystal violet in the presence of hydrogen peroxide. Deposition of sufficient amount of iron oxide particles on textiles enabled their simple magnetic separation from large volumes of solutions; if necessary, the magnetic response of the modified textiles can be simply increased by incorporation of a piece of magnetic iron wire. The simplicity of immobilized nanozyme preparation and low cost of all the precursors can enable its widespread application, such as decolorization and degradation of selected organic dyes and other important pollutants. Other types of textile-bound nanozymes can be prepared and used as low-cost catalysts for a variety of applications.

1.   Introduction

Magnetic iron oxide nano- and microparticles have a great potential in biochemical, biomedical, clinical, biotechnology and environmental applications owing to their many unique properties [1-2]. These biocompatible nanoparticles exhibit several types of responses to external magnetic fields, namely selective separation, targeting and localization of magnetically responsive nano- and microparticles and other relevant materials using an external magnetic field (represented e.g. by permanent magnets, electromagnet or appropriate magnetic separators) [3],

heat generation caused by magnetic particles subjected to high frequency alternating magnetic field [4], increase of a negative T2 contrast by magnetic iron oxide nanoparticles during magnetic resonance imaging [5], formation of "hot spots" during magnetic particle imaging [6] or great increase of apparent viscosity of magnetorheological fluids when subjected to a magnetic field [7].

In the year 2007 a new property of magnetic iron oxide nanoparticles was described, namely the presence of intrinsic peroxidase-like (P-L) activity similar to horseradish peroxidase (HRP); this was the first time an inorganic nanoparticle was considered as an enzyme mimetic for potential biomedical applications [8]. The term "nanozyme" was introduced to define nanomaterials with intrinsic enzyme-like activities [9].

Iron oxide nanozymes (IONs) including Fe_3O_4 and Fe_2O_3 nanoparticles are currently the most typical enzyme mimetic materials which have been used for many applications. Their P-L activity has been observed during the typical colorimetric reaction involving hydrogen peroxide (H_2O_2) and appropriate chromogenic reagents. This P-L activity requires similar optimal conditions as those for HRP, including the optimal temperature at 37-40 °C under the optimal pH (pH 3-6.5) in an acidic buffer [9]. Combination of IONs with glucose oxidase enabled detection of glucose [10]; alternatively, other oxidases that generate H_2O_2 as an intermediate can be integrated with IONs to detect corresponding substrates including cholesterol oxidase for cholesterol [11], galactose oxidase for galactose [12], and alcohol oxidase for alcohol [13].

Both naked iron oxide nanoparticles [8] and those entrapped in biopolymer matrices [14] exhibit P-L activity. Immobilization of (bio)catalysts to an appropriate solid carrier enables their simple separation from the reaction mixture and repeated applications. There are many different methods used for (bio)catalyst immobilization [15-16], but usually simple, cost-effective and green

methods are preferred. The most used methods are based on physical immobilization (adsorption or physical entrapment) and chemical immobilization (covalent binding and cross linking) [17].

Textile materials represent low-cost carriers that exhibit several other material-inherent advantages such as flexibility, mechanical strength and high surface area [18]. Textile materials have been efficiently used for immobilization of affinity ligands [19], polysaccharides [20], ionic liquids [21], enzymes [18, 22] or (nano)particles [23-25]. For example, manganese dioxide microparticles adsorbed on non-woven fabric fibers were used as a recoverable catalyst for hydrogen peroxide decomposition [26] while textile modified with silver nanoparticles exhibited antibacterial properties [23]. Recently different types of textile materials were modified by iron oxide (nano)particles or microfibers to obtain composites exhibiting interesting properties, such as electromagnetic shielding [27-28], removal of important pollutants from water sources [29], degradation of selected organic dyes [30], possibility of immobilization of biologically active compounds and cells [31] or to prepare new types of colored textiles [32]. In specific cases simultaneous magnetic, photocatalytic, sonocatalytic, antibacterial and antifungal activities have been found in iron oxide modified textile [33]. A recent review chapter summarizes magnetic nanofinishes for textiles in detail [34]. Alternatively, magnetically responsive textile composite (bio)catalysts or adsorbents for magnetic textile solid phase extraction can be prepared by the insertion of a piece of magnetic iron wire in the textile material in order to simplify their rapid recovery from the reaction mixture or analyzed solution [19-20, 26].

In the present study, iron oxide nanozyme particles were attached to a cotton textile using two simple procedures, employing either water based magnetic fluid stabilized with perchloric acid, or magnetite nanoparticles prepared by microwave assisted synthesis. The latter approach is especially important because magnetic iron oxide particles are prepared in an extremely easy

way from a single ferrous salt (usually ferrous sulfate at high pH) using a standard domestic microwave oven [35]. Both modified textiles exhibited peroxidase-like activity and exhibited decolorization activity for selected organic dyes; also efficient and low-cost degradation of other aromatic compounds (phenols, bisphenols, anilines) generated by a variety of industries can be expected. Magnetic properties of the modified textiles allowed for a simple magnetic separation from the reaction mixtures. The detailed characterization of the modified textile was performed using scanning electron microscopy (morphology and structure of native and magnetically modified textile materials) and by vibrating sample magnetometer installed on a cryogen-free superconducting magnet (basic magnetic properties of the investigated materials). In order to characterize the structure of the modified textiles on the nanometer scale, small-angle X-ray and neutron scattering (SAXS and SANS) measurements have been performed.

2. Materials and methods

2.1. Materials

FeSO$_4$. 7H$_2$O, NaOH, crystal violet (Basic violet 3; Color Index No. 42555; CV) and hydrogen peroxide were obtained from Sigma-Aldrich, Czech Republic. N,N-diethyl-p-phenylenediamine sulfate salt (DPD) was purchased from Merck, Germany. Water-based magnetic fluid (MF) stabilized with perchloric acid was prepared using a standard procedure [36]; the iron oxide concentration was 36.0 mg mL^{-1}. Cotton textile (white fine plain-woven canvas, 100 g m^{-2}) was obtained locally; before use it was repeatedly boiled in distilled water and after drying squares of 2x2 cm size were cut. Domestic kitchen microwave oven (700 W, 2 450 MHz), as well as an office stapler and common iron-based staples were obtained locally.

2.2. Microwave assisted modification of cotton textile

For the first type of modification, cotton squares (2x2 cm) were saturated with 100 μL FeSO$_4$. 7H$_2$O solution (concentrations ranges between 0.2 and 20 % (w/vol)) and dried at 50 °C till complete dryness. Ten textile squares containing dried ferrous sulfate were added to a 1 L beaker containing 2 % NaOH solution (250 mL) and the content was microwave (MW) treated (boiled) in a kitchen microwave (700 W) for 10 min at the maximum power. Modified textile squares were 2-times washed with excess of water and dried at room temperature (22 °C) till complete dryness. For comparison, a suspension of iron oxide nanoparticles was prepared from ferrous sulfate at high pH under MW irradiation as described [35, 37].

2.3. Ferrofluid modification of cotton textile

In the second procedure, the textile square modification was performed with perchloric acid stabilized magnetic fluid diluted with methanol to final concentrations in the range between 0.001 mg mL^{-1} and 10 mg mL^{-1}; in all cases 100 μL of the nanoparticle solutions were applied on the textile squares (2x2 cm) that were then dried at room temperature (22 °C) till complete dryness.

2.4. Determination of peroxidase-like activity

The peroxidase-like activity of both types of modified textile materials was determined in a reaction mixture containing 3.4 mL of deionized water, 400 µL of DPD solution (12.53 mmol L^{-1}) and 200 µL of 2% H_2O_2. The reaction was initiated by addition of 2x2 cm modified cotton textile samples in the reaction mixture. The samples were incubated under mixing at room temperature (22 °C) for 5 min. The absorbance at a wavelength λ of 551 nm was measured [38] using a Cintra 20 spectrophotometer (GBC Scientific Equipment, Braeside, Australia) and then the absorbance of the corresponding blank containing all of the reagents except the tested samples was subtracted. All measurements were performed in triplicate and arithmetic means and standards deviations were calculated.

2.5. Decolorization of crystal violet

Crystal violet solution (4 mg L^{-1}, 4.83 mL) and 170 µL of 30% hydrogen peroxide (to study nanozyme-based decolorization of CV) or water (to study adsorption of CV to modified textile) were added into 10 mL test tubes. Cotton textile squares (2x2 cm) modified with microwave synthesized iron oxides (prepared from 100 µL of 10% $FeSO_4$. $7H_2O$) were inserted into the dye solutions and absorbance at λ = 551 nm was measured. Three decolorization experiments were performed at room temperature (22 °C).

2.6. Small-angle X-ray scattering

SAXS measurements were performed at the BioSAXS beamline P12, EMBL/DESY, Hamburg, Germany [39], using the 150 µm (v) x 250 µm (h) X-ray beam at an X-ray energy of E = 10 keV (wavelength λ = 0.124 nm). Two-dimensional SAXS patterns were recorded using a PILATUS 6M pixel detector [40] at a sample-detector-distance of 4 m, covering the range of momentum transfer q = 0.02 – 5.5 nm^{-1} (q = $4\pi/\lambda$ sin(Θ), where 2Θ is the scattering angle).

SAXS data were collected from the different nanoparticle-modified textiles and unmodified cotton textile as reference. Scattering patterns were recorded from several spots on the specimens to check for sample homogeneity. In addition, suspensions of both types of iron oxide nanoparticles in water were measured as well. The suspensions were filled into quartz glass capillaries (Hilgenberg, Germany; outer diameter: 1.50 mm, wall thickness: 0.01 mm) and placed within a custom-made capillary holder. As reference measurement, the scattering signal from pure water filled into a capillary was collected.

For the cotton textile and for some of the composite specimen, the 2D scattering patterns are anisotropic close to the primary beam at small angles due to the microstructure of the cotton fibers and change for different spots on the sample. For momentum transfers of q > 0.1 nm^{-1}, however, there are no differences between the patterns, which motivated us to perform the azimuthally averaged SAXS profile (masking inter-module segments of the detector as well as the shadows of the beam stop and the flight tube) using the P12 beamline SASFLOW pipeline [41]. 1D SAXS curves of each sample were scaled to correct for differences in the sample thickness, compared for similarity and averaged. From these 1D-SAXS profiles the scattering signal recorded without sample (air scattering plus instrumental background) was subtracted. For the

nanoparticle suspensions, the isotropic scattering patterns were as well azimuthally averaged, and the scattering of water was subtracted.

All SAXS curves were further analyzed using the ATSAS software package [42]. The pair-distance distribution functions from the scattering profiles were computed with the ATSAS program GNOM [43].

2.7. Small-angle neutron scattering

SANS measurements were carried out using the small-angle spectrometer YuMO at the IBR-2 pulsed reactor (JINR, Dubna, Russia) in the time-of-flight mode [44]. The SANS scattering curves were obtained using a wavelength range of 0.05 – 0.8 nm. Samples were placed in plain quartz cuvettes with the optical path length of 2 mm. The absolute calibration of the scattered intensity was made using vanadium standard. Finally, the raw data were averaged using the SAS program [45].

The analysis of the SANS curves was performed using SasView software [SasView version 4.0, http://www.sasview.org/] and Indirect Fourier Transform (IFT) method developed by Glatter [46] in the version of Pedersen [47] was also applied.

2.8. Magnetic characterization

The magnetic properties of the textile materials were characterized by using a vibrating sample magnetometer (Cryogenic Limited, UK) and an AC susceptometer (Imego Dynomag, SE). The

magnetization curves were measured at room temperature (298 K) and static magnetic field up to 5 T. The specific mass magnetization was calculated as a ratio of the measured magnetic moment (emu) and the sample mass (g). The AC magnetic susceptibility was measured in the frequency range from 1 Hz up to 250 kHz. The amplitude of the excitation AC magnetic field intensity is 400 A m^{-1}. For this measurement, the textile of a precisely measured mass was placed in a glass cuvette, for which a background signal was subtracted in the calibration procedure.

2.9. Further characterization

The morphology and structure of native and magnetically modified textile materials was studied by scanning electron microscopy (SEM). Samples were analyzed using a Hitachi SU6600 scanning electron microscope (Hitachi, Tokyo, Japan) with accelerating voltage 1.5, 3 or 5 kV. Energy dispersive X-ray spectra (EDS) were acquired in SEM using Thermo Noran System 7 (Thermo Scientific, Waltham, MA, USA) with Si(Li) detector; the accelerating voltage was 15 kV and the acquisition time was 300 s.

3. Results and discussion

3.1. Magnetic iron oxide nanoparticles deposition on cotton textile

Two simple modification procedures (previously used by the first author and his colleagues for magnetic modification of a wide variety of diamagnetic organic, inorganic, and biological particulate and high aspect ratio materials [3, 48-50]) were employed to prepare cotton textile squares

loaded with magnetic iron oxide nanoparticles; several batches of each type were prepared. In the first case each cotton square was saturated with $FeSO_4 . 7H_2O$ solution of different concentration and subsequently microwave treated to convert ferrous salt into magnetic iron oxide nanoparticles and their aggregates [35, 37]. The cotton textile damage was negligible using visual and optical microscopy observation when microwave heating of plain textile in sodium hydroxide solution used was tested. In the second case the textile squares modification was performed with perchloric acid stabilized magnetic fluid of different concentration; for magnetization measurements of MF see Figure S1 in the Supporting Information. All the modified textile squares exhibited light to dark brown color depending on the amount of bound iron oxide particles and this color of the modified textile is fully correlated with the magnetic particle concentration (Fig. 1). The binding of magnetic nanoparticles to textile was strong and almost no leakage of nanoparticles was observed during storing the modified textile in water or during the decolorization experiments.
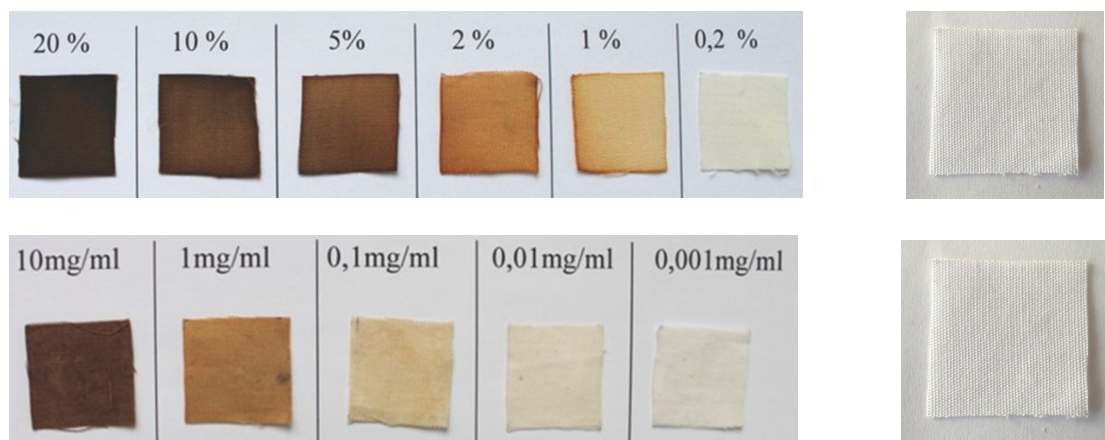
Figure 1. Appearance of cotton textile squares modified with microwave-synthesized magnetic iron oxide particles (top; concentrations (w/v) of $FeSO_4 \cdot 7H_2O$ solutions are presented) and perchloric acid stabilized ferrofluid in methanol (bottom; concentrations of iron oxide nanoparticles in FF are presented). In all cases 100 µL of solutions were applied on 2x2 cm cotton textile squares. Native cotton textile is on the right.

For detailed characterization, cotton textile samples modified with 20 % ferrous sulfate solution under microwave irradiation and ferrofluid modified textile (FF concentrations 10 and 1 mg mL^{-1}) were used. SEM of native and modified textile squares clearly showed the presence of iron oxide nanoparticles on the surface of the modified cotton fibers (Figure 2). Most nanoparticles prepared by microwave assisted synthesis had diameters between 50 and 150 nm as revealed by SEM which corresponds to previous study [37]; on the contrary most individual nanoparticles originating from acid ferrofluid had smaller diameters varying between 10 and 20 nm. The micrographs show that there are areas with a continuous layer of iron oxide nanoparticles on the textile fiber and areas where these nanoparticles are present individually or in the form of rather dense aggregates.
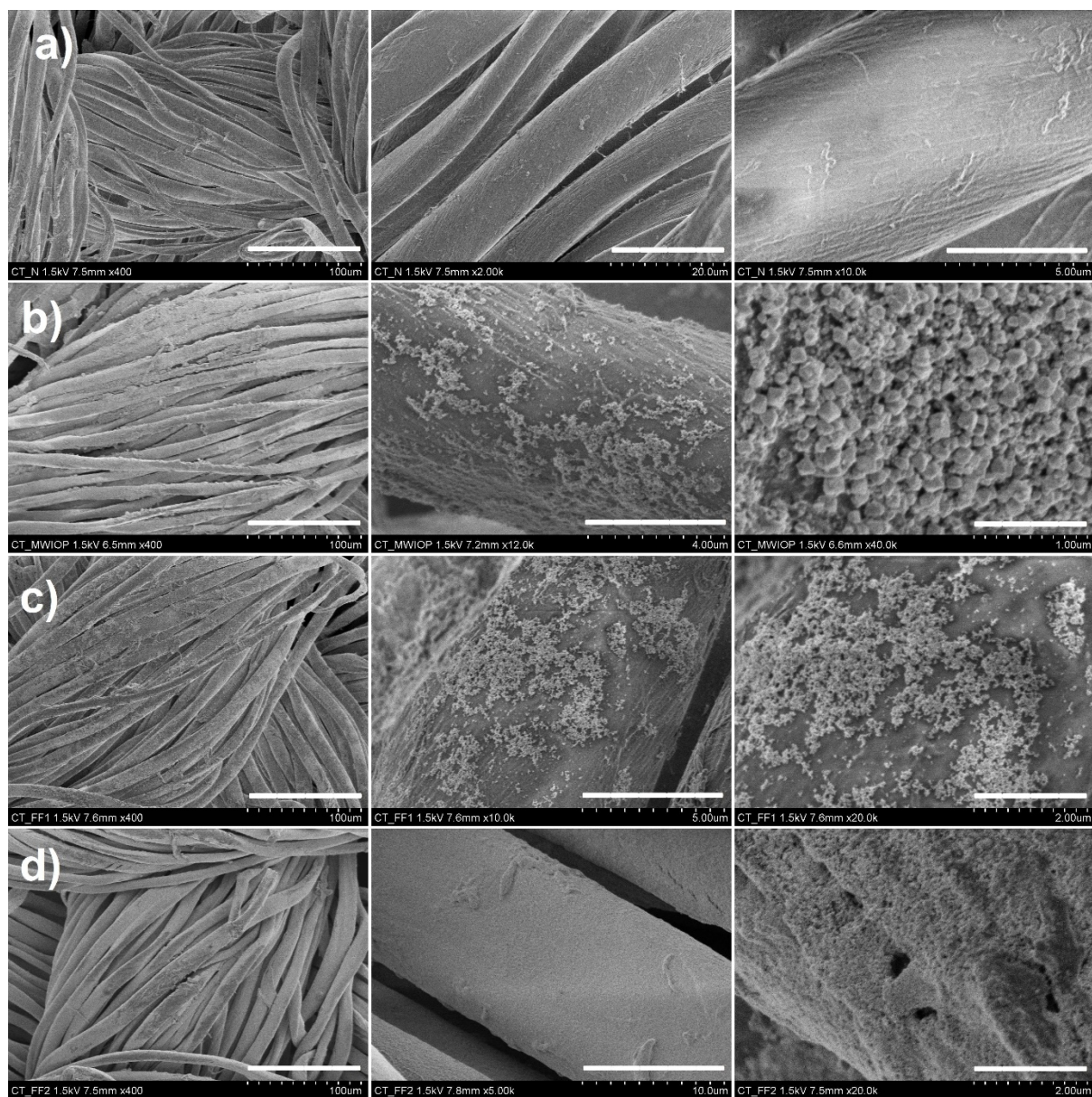
Figure 2. SEM images of a) native cotton textile (400, 2000 and 10000 times magnification; bars 100, 20 and 5 µm), b) cotton textile modified by microwave irradiation (20 % $FeSO_4 \cdot 7H_2O$ solution used; 400, 12000 and 40000 times magnification; bars 100, 4 and 1 µm), c) cotton textile modified with acid FF (concentration 1 mg mL^{-1} used; 400, 10000 and 20000 times magnification; bars 100, 5 and 2 µm) and d) cotton textile modified with acid FF (concentration 10 mg mL^{-1} used; 400, 5000 and 20000 times magnification; bars 100, 10 and 2 µm).

The successful synthesis and deposition of iron oxide nanoparticles on the modified textiles was also confirmed by EDS; typical iron peaks at 0.705, 6.398 and 7.057 keV are present in the iron oxide modified textile samples (Figure S2, see the Supporting Information).

Deposition of sufficient amount of iron oxide particles on the textile squares allowed the simple magnetic separation from large volumes of solutions; if necessary, the magnetic response can be simply increased by incorporation of a piece of magnetic iron wire, such as an iron office staple (see Figure 3).
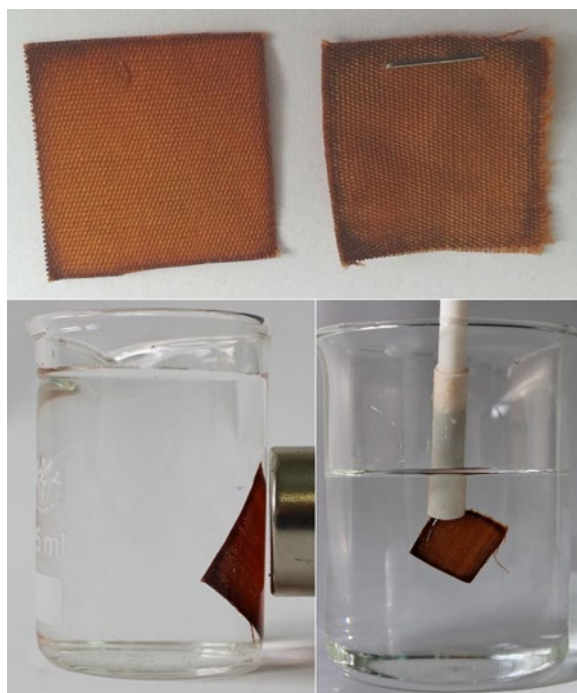

Figure 3. Magnetic separation of FF modified textile (FF concentration 10 mg mL^{-1}) without (left) and with inserted magnetic iron staple (right).

Both the microwave-assisted modification procedure and ferrofluid treatment have been also successfully employed previously for magnetic modification of other types of textile from both natural and synthetic fibers, in addition to various biological, inorganic, and organic particulate and high aspect ratio materials [49-50]. This indicates that most probably the mechanism of magnetic nanoparticles binding to diamagnetic materials is not based on the creation of new covalent bonds involving the functional groups of the modified material. It can therefore be concluded that physical adsorption is responsible for magnetic nanoparticles binding to the textile fibers; also hydrogen bonding between iron oxide nanoparticles and cellulose chains can be involved [51]. In the specific case of nanoparticle-modified woven textile the nanoparticles can also be deposited or trapped between the warp and weft yarns, within the yarns, or inside the nanoscale interstices of cellulose fibers, depending on their size and concentration. The same situation was observed in the case of coating of silver [52-53] or titanium dioxide [54] nanoparticles on textile materials.

3.2. Magnetic characterization

Magnetic characterization of the textiles modified with magnetic nanoparticles was performed. The magnetization curves measured on the studied samples at room temperature are presented in Figure 4. For each curve, zero hysteresis is found, so revealing the superparamagnetic nature of the magnetic nanoparticles. One can clearly see that the magnetizations are well saturated already at 1T. The values of saturation magnetization are reflecting the quantity of magnetic nanoparticles present in the textiles. The textile modified with 20 % ferrous sulfate solution under microwave irradiation (MW 20%) exhibits magnetization of saturation 4.34 emu g^{-1}, while

the textiles modified with FF of 10 mg mL^{-1} (FF 10 mg mL^{-1}) and 1 mg mL^{-1} concentration (FF

1 mg mL^{-1}) show magnetization of saturation 3.64 emu g^{-1} and 0.49 emu g^{-1}, respectively. Then,

the quantity of magnetic nanoparticles (magnetic mass fraction) can be determined as a ratio of

the found magnetization of saturation to the domain magnetization of the nanoparticles [55-56].

Considering the domain magnetization of magnetite [57] (86.2 emu g^{-1}), one gets the following

magnetic mass fractions 5.03%, 4.22% and 0.57% for MW, FF 10 mg mL^{-1} and FF 1 mg mL^{-1},

respectively. Owing to the relatively high concentration of magnetic nanoparticles in the textiles

(especially MW 20% and FF 10 mg mL^{-1}), the positive magnetization dominates the total

magnetization of the modified textiles and the diamagnetic contribution from the pure textile is
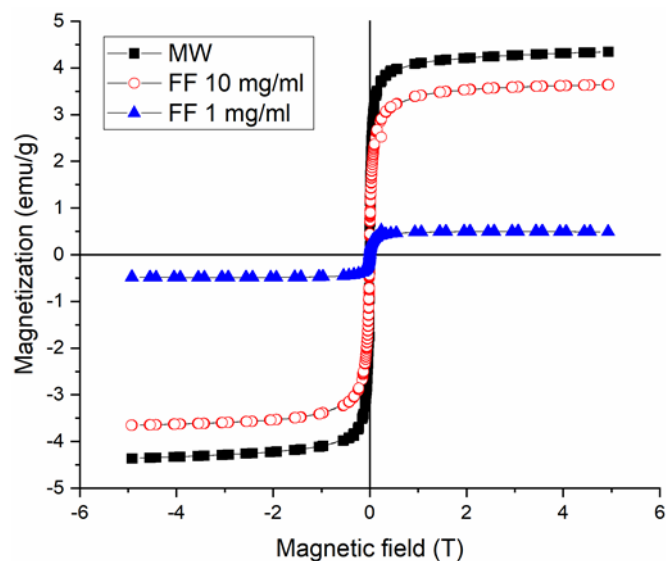
negligible.

Figure 4. Magnetization curves measured at room temperature (298 K). MW – cotton textile modified by microwave irradiation using 100 µL of 20% $FeSO_4 . 7H_2O$; FF 10 mg/ml – cotton textile modified with 100 µL of magnetic fluid (10 mg mL^{-1}); FF 1 mg/ml – cotton textile modified with 100 µL of magnetic fluid (1 mg mL^{-1}). Five measurements were performed; the error bars are smaller than the symbols representing the data points.

In Figure 5, the spectra of AC magnetic real susceptibility are presented. One can clearly see that the susceptibility values for MW 20% and FF 10 mg mL^{-1} are significantly greater than for FF 1 mg mL^{-1}. This is associated with the magnetic nanoparticle concentration, which is one order of magnitude greater for MW 20% and FF 10 mg mL^{-1}, as compared with FF 1 mg mL^{-1}. As a result, FF 1 mg mL^{-1} yielded a very weak AC magnetic signal in the low AC excitation magnetic field. The signal is apparently close to the sensitivity limit of the device's detection system and therefore the calculated real AC susceptibility of FF 1 mg mL^{-1} is around zero in the whole frequency range. For MW 20% and FF 10 mg mL^{-1} a moderate decrease in susceptibility

with increasing field frequency is observed. However, the spectra do not show any clear dispersion corresponding to a particular relaxation process. As the nanoparticles are confined in the textile, their magnetic moments cannot respond the AC magnetic field via Brownian relaxation. Thus, only Néel relaxation mechanism is supposed to contribute to the real magnetic susceptibility. Then, the decreasing susceptibility with increasing field frequency reflects the polydispersity in the nanoparticle size. One can consider that larger nanoparticles contribute to the susceptibility at lower frequencies. At higher frequencies, the moments of greater nanoparticles are not able to follow the field changes as the Néel relaxation time is exponentially dependent on the magnetic anisotropy energy and therefore on the nanoparticle volume as well.
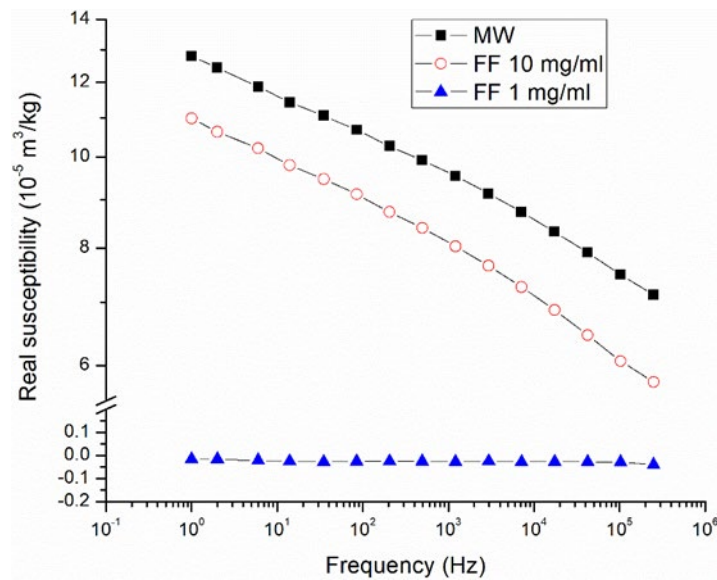

Figure 5. Real part of AC magnetic susceptibility in dependence on the frequency of the external magnetic field. For legends see Figure 4. Five measurements were performed; the error bars are smaller than the symbols representing the data points.

19

3.3. Structural characterization at the nanoscale

Small-angle X-ray and neutron scattering measurements were conducted for the detailed structural characterization at the nanoscale of both types of textiles: the textile modified with 20 % ferrous sulfate solution under microwave irradiation as well as the ferrofluid modified textiles (FF concentrations 10 and 1 mg mL^{-1}). The simultaneous application of X-rays and neutrons gives the advantage to improve quite low statistic and resolution function of SANS and to enlarge the field of view and omit possible radiation damage of SAXS. Experimental SAXS and SANS curves are presented in Figure 6. The small-angle scattering (SAS) signal from the magnetic nanoparticles dominates in both SAXS and SANS measurements for both textile types due to the higher scattering contrast compared to cotton. As it is clearly seen from Figure 6, all SAS curves for the initial unmodified cotton and textiles modified by NPs exhibit a power-law decay at small q-values, reflecting the presence of large, extended structures. For the modified textiles, the SAS curves are changing with addition of MNPs, indicating the formation of various structures at the nanoscale. In particular, the shoulder in the range 0.1 nm^{-1} < q < 1.0 nm^{-1} can be associated with the NPs.

It should be noted that the SAXS and SANS profiles are similar in the overlapping q-regions after correspondingly scaling of intensity (see Figure S3 in Supporting Information). Multiplication factors are different which is probably due to some non-homogeneity through the sample surface and different raw data treatment procedures for the SAXS and SANS data.
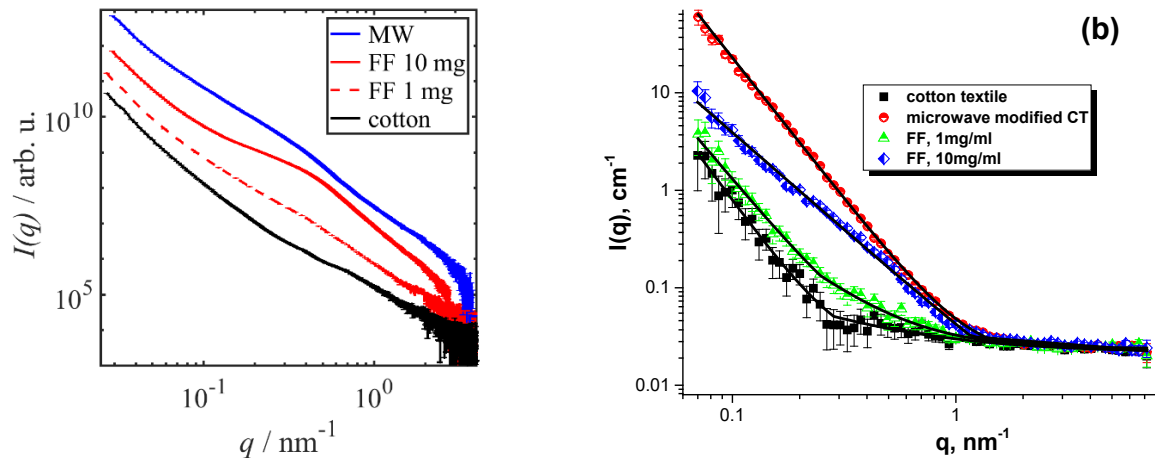
Figure 6. Experimental SAXS (a) and SANS (b) profiles for initial unmodified cotton and nanotextiles modified by MNPs (for legends see Figure 4). Solid lines on (b) correspond to power-law fit.

As reported in previous studies, the nanostructure of cotton fibers consists of cellulose microfibers which can be approximately described by very long cylinders [58]. In order to quantify the cross-sectional dimension for the presented cotton specimen, we determined the cross-sectional pair-distance distribution function $p_{cs}(r)$ (Figure 7b). It reflects the circular shape of the microfiber cross-section with a cross-sectional radius of gyration of $R_{g,cs} = 3.0 \pm 0.2$ nm and a maximum diameter of $d_{max} = 9.3$ nm. As the scattering contribution of cotton is much smaller than those for the modified textiles (in particular in the mid q-range), the scattering signal of cotton was subtracted from the other SAS data (Figure 7a and 7c). This approach was motivated by the fact, that the nanoparticles presumably are adsorbed on the cotton matrix without any obvious additional interference effects present (as also suggested by the SEM images), and thus the scattering from cotton can be treated just as an additional background contribution. Such

subtracted curves are shown on Figure 7a and 7c, which basically reflects the scattering of the adsorbed nanoparticles. It should be mentioned that power law exponents at the SANS data (Figure 7c) are increased with increasing of MNPs concentration for the ferrofluid modified textiles and are even higher for MNP sample with microwave-assisted synthesis. It points out to more dense formation of the MNPs aggregates in the corresponding samples.

The comparison of the SAXS curves for the nanoparticles in suspension with those adsorbed on the textiles is presented in Figure 7a. As can be clearly seen, the textiles for the diluted ferrofluid sample (FF 1 mg mL^{-1}) strongly resembles the SAXS profiles from the ferrofluid suspension, in particular at large q. A detailed analysis for the structure of NP in suspension can be found in Figure S4 in the Supporting Information. In short, both suspensions (ferrofluid and MNPs from microwave-assisted synthesis) consist of two particle species, namely small particles and large aggregates formed from the smaller ones. In particular, elongated aggregates (size: 170 nm) are present for the ferrofluid suspension, which have been observed also previously [59]. The data for the textiles with FF 1 mg mL^{-1} thus suggest that dominantly the small single spherical particles of 17 nm size are adsorbed on the cotton matrix independently.

For increasing ferrofluid concentration up to 10 mg mL^{-1}, an additional shoulder appears with position around $q_{corr} \approx 0.5$ nm^{-1} for both SAXS and SANS data, which indicates interparticle correlation distances $d_{corr} = 2\pi/q_{corr} \approx 13$ nm and its close to the single particles size, i.e. closely touching particles with radius of gyration ~ 5 nm. At the small q-region, the curve decays with a power law exponent of $\sim$ -1.5, similar to that of mass-fractal particles [60], pointing to a connected network of particles adsorbed on the cotton matrix forming an overall elongated structure. In more detail, this SAXS data for MNP adsorbed from a 10 mg mL^{-1} FF suspension can be as well described by an indirect Fourier analysis of infinitely long rods. The maximal size of the *p(r)*

function of the smaller particles of MNPs suspension (analyzed as 3-dimensional object, see Figure S4 in the Supporting Information) is equal to the maximal size of the cross-sectional $p_{cs}(r)$ of MNPs adsorbed to the cotton fibers (analyzed as cross section of infinitely long cylinder, 2dimensional object). It corresponds roughly to the diameter of single MNP. Based on this we can conclude that single MNPs adsorb to the cotton and form elongated (rod-like) complexes following the cotton fiber matrix.

For MW treated textiles, the MNP particles exhibit a different structure compared to that of the suspension prepared by a standard procedure from ferrous sulfate at high pH [35] (see analysis of suspension in the Supporting Information). The decay exponent is ~ -2.7 to - 2.9, which is more similar to volume fractal like structures. Analysis of the microwave-based particles with the same indirect Fourier analysis of infinitely long rods gives the $p_{cs}(r)$ of a larger particle than for FF MNPs adsorbed to cotton and with a maximal size d_{max} that corresponds to complexes of 3-4 single MNPs for MW-based suspension.
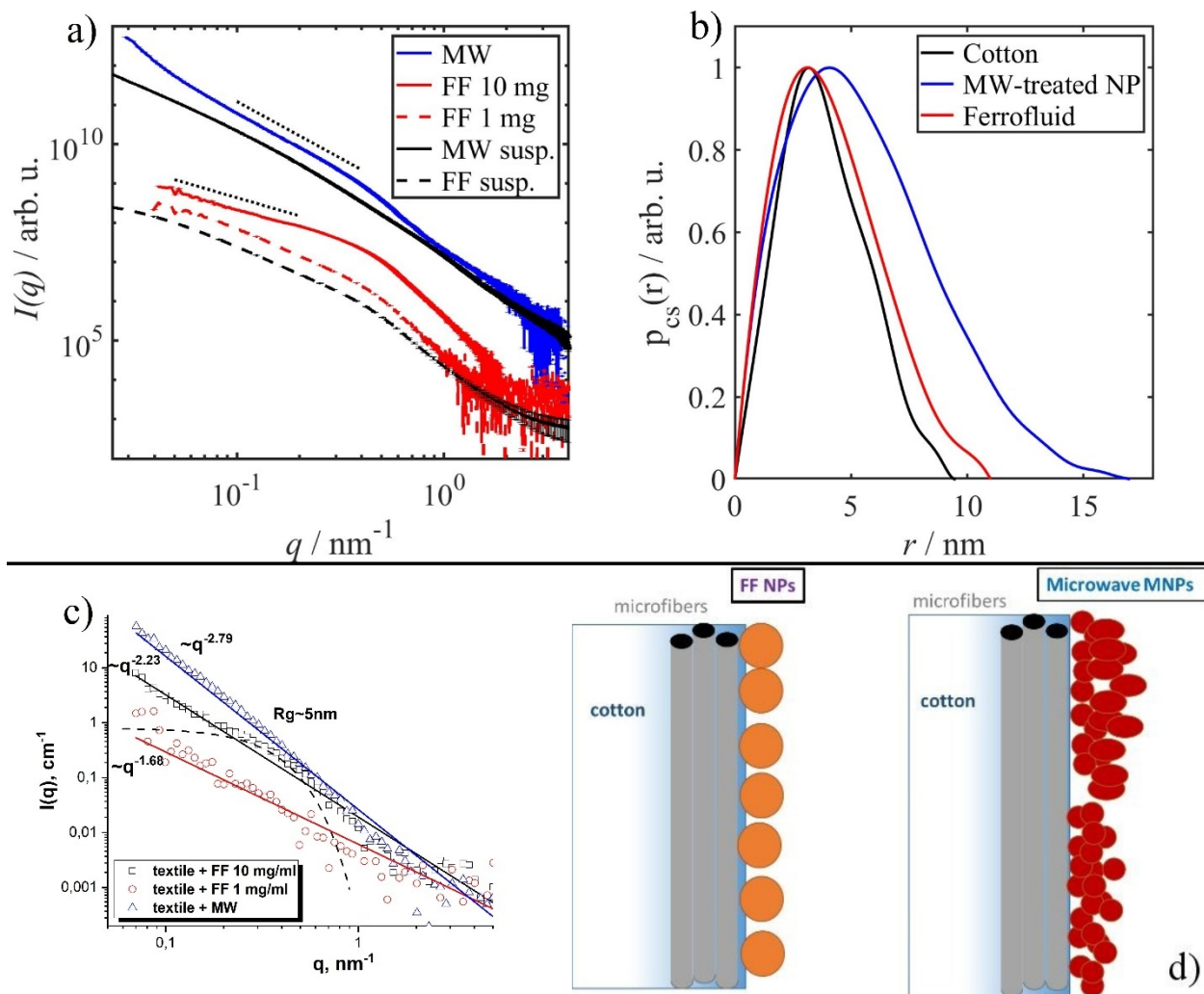
Figure 7. (a) SAXS curves after subtraction of the cotton signal (microwave (MW) and ferrofluid (FF) treated textiles). The scattering profiles from both types of nanoparticles in suspension are also shown. Dotted lines: power law fits. All curves were shifted vertically for clarity. (b) Cross-sectional distance distribution function $p_{cs}(r)$ determined from the cotton data and the subtracted nanoparticle data. (c) SANS curves for the modified nanotextiles after subtraction of the initial cotton signal. Solid lines: power law fit with corresponding exponents values. Dotted line is Guinier curve with the mentioned gyration radius. (d) Sketch of the proposed MNPs organization in modified nanotextile according to the SAXS data. For legends see Figure 4.

Figure 7b compares the cross-sectional distribution functions of infinite rods for both samples of adsorbed nanoparticles to characterize the morphology of the adsorbates as well as of the cotton matrix. For the ferrofluid, $p_{cs}(r)$ exhibits the shape characteristic of a circular cross-section and d_{max} = 11 nm, which is similar to the size of the single nanoparticle in the ferrofluids. For the MW-based sample, the curve is slightly broader and as d_{max} = 17 nm is larger than for the size of the respective single particle, this indicates the adsorption of aggregates of MNPs on cotton.

Based on the small-angle analysis of the nanostructures, ferrofluid particles adsorb roughly as a single layer of smaller nanoparticle in close contact. With increasing concentration, the layer gets denser. The particle shape is identical to that for the suspension. In contrast, the synthesis approach for the MW-treated samples appears to have changed the sample structure. For the studied sample, a relative dense structure of a few layers of nanoparticles has formed. The proposed sketch of MNPs adsorption on the cotton fibers is presented on Figure 7d. This model is solely based on the scattering data, which probe the textiles over a large area. It is consistent with the SEM images from local spots, providing a unified picture of the micro-and nanostructure over the whole sample size.

3.4. Nanozyme properties of textile bound iron oxide particles

Iron oxide particles are well known nanozymes exhibiting peroxidase like activity [8]. Immobilization of nanozyme particles on magnetically responsive carriers enables their simple separation from large reaction volumes or from difficult-to-handle samples. Nanozyme or inorganic catalysts (nano)particles immobilized on magnetically responsive textile prepared by insertion of magnetic iron wire [26] are of special interest due to their low cost, simple preparation

and subsequent manipulation (see Figure 3). The herein studied textile bound iron oxide particles exhibited typical peroxidase-like response after interaction with a standard peroxidase substrate (DPD) in the presence of hydrogen peroxide as presented in Figure 8; originally colorless DPD was oxidized to a colored product with a strong absorption maximum at 551 nm [38, 61].
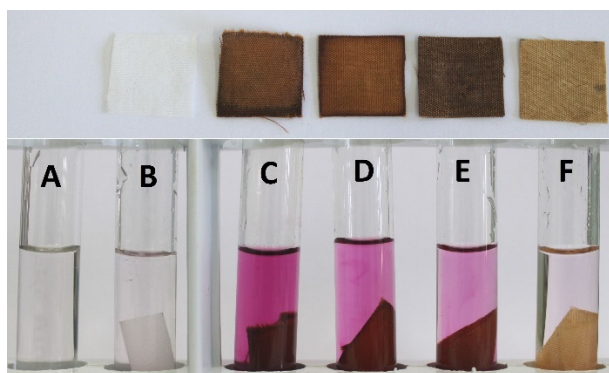

Figure 8. Peroxidase-like activity of iron oxide modified textile squares employing DPD as the substrate. From left to right: A - reaction blank; B - native cotton textile; C - textile modified with 20 % $FeSO_4 . 7H_2O$; D - textile modified with 10 % $FeSO_4 . 7H_2O$; E - textile modified with FF (10 mg mL^{-1}); F - textile modified with FF (1 mg mL^{-1}).

The amount of textile-bound iron oxide particles influenced the measured peroxidase-like activity. Table 1 presents the average PL activities (represented as absorbance changes at 551 nm from three independent measurements and subsequently converted into catalytic activity in nanokatals) per 1 cm^2 of the iron oxide modified cotton textile.

Table 1. Peroxidase-like activity of textile-bound iron oxide particles (nkat cm^{-2})

Type of iron oxide modified textile	P-L activity [nkat cm^{-2}]
MW, 1% FeSO$_4$. 7H$_2$O	20.8 ± 1.2
MW, 2% FeSO$_4$. 7H$_2$O	28.5 ± 1.4
MW, 5% FeSO$_4$. 7H$_2$O	43.7 ± 1.9
MW, 10% FeSO$_4$. 7H$_2$O	56.9 ± 2.3
MW, 20% FeSO$_4$. 7H$_2$O	77.8 ± 2.9
FF, 1 mg mL^{-1}	3.9 ± 0.2
FF, 10 mg mL^{-1}	38.0 ± 1.5

The decolorization of water-soluble organic dyes and degradation of a wide spectrum of aromatic compounds (phenols, biphenols, anilines) generated by a variety of industries is a main issue in wastewater treatment. Natural enzymes peroxidases (EC 1.11.1.x) are hemoproteins that catalyze reactions in the presence of hydrogen peroxide. Heme peroxidases are a ubiquitous family of enzymes produced by almost all organisms. Both native and immobilized peroxidases have been often tested for organic dye decolorization [62-63]. Decolorization of Remazol blue and crystal violet [64], bromophenol blue and methyl orange [65] and Remazol Turquoise Blue G and Lanaset Blue 2R [66] by peroxidases in the presence of hydrogen peroxide can serve as typical examples. However, the production of target enzymes can be expensive, and the enzyme can be inhibited in the presence of the treated dye. These facts present the major limitations in potential

commercial application of the technique for effluent treatment in the dye manufacturing industry [64].

However, recently discovered nanozymes exhibiting peroxidase-like activity could solve this problem. They may offer the potential bioremediation ability towards a broad range of toxic, carcinogenic and hazardous environmental pollutants at low cost. Peroxidase-like activity of textile bound iron oxides enabled decolorization of selected organic dyes including crystal violet (CV). CV is a triphenylmethane dye widely used in the textile production or in paper factories; it has also antimicrobial, antifungal and antiparasitic properties. In addition, CV is toxic to mammalian cells and exhibits mutagenic properties [67]. Due to the all above mentioned facts CV is a very often used model dye to study enzyme-based decolorization processes. As shown in Figure 9, quite rapid CV decolorization in the presence of hydrogen peroxide was observed using textile bound iron oxide particles prepared by microwave assisted synthesis; this textile composite can be prepared in a simple way from low-cost precursors and could be potentially employed for larger-scale applications. Almost colorless solution was obtained after 10 min reaction under experimental conditions. Of course, adsorption of CV on iron oxide modified textile was investigated to ascertain that decolorization of dye is mainly caused due to oxidative action of iron oxide based nanozyme. Figure 9 shows that CV has partially adsorbed on the modified textile when no hydrogen peroxide was present in the reaction mixture; anyway, the nanozyme based decolorization in the presence of hydrogen peroxide played a dominant role. Due to the simplicity of the catalyst (nanozyme) preparation and extreme low cost of all the precursors there is no need for catalyst regeneration and subsequent repeated application. In addition, application of magnetically responsive textile carrier (due to the incorporation of a piece of magnetic iron wire) for the nanozyme or other catalyst deposition enables very rapid

recovery of the immobilized catalyst from large volume of the reaction mixture. Both factors

represent a great advantage of the described textile-based nanozyme composite in comparison

with an alternative described procedure where complex process has been used to prepare

magnetic nanoparticles incorporated in a cellulose matrix [68]. It should be mentioned that the

ferrofluid modified textile exhibited similar decolorization properties.
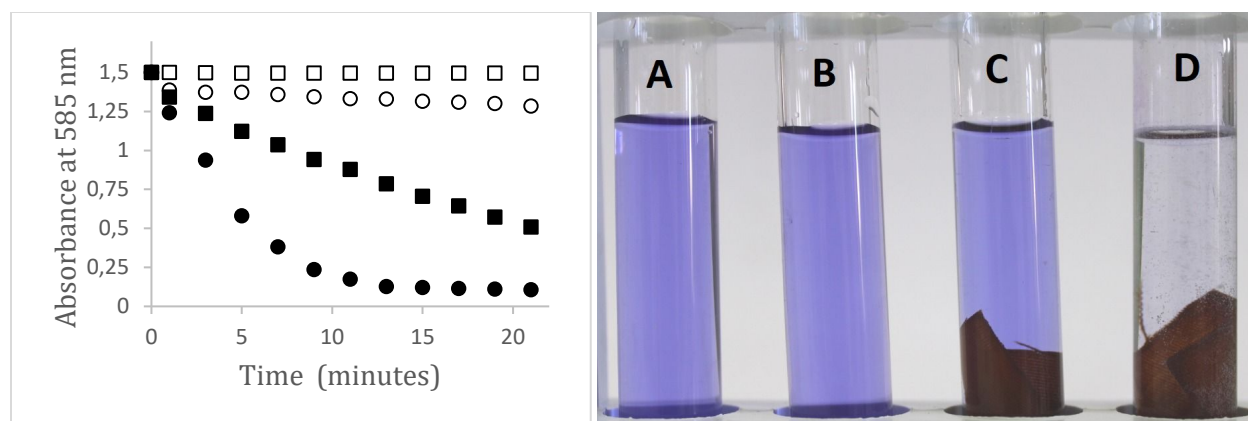

Figure 9. Left - decolorization of crystal violet. □ - CV + H_2O (test tube A); ○ - CV + H_2O_2 (test

tube B); ■ - CV + H_2O + cotton textile modified with microwave synthesized iron oxides (test

tube C); ● - CV + H_2O_2 + cotton textile modified with microwave synthesized iron oxides (test

tube D). Three decolorization experiments were performed; the error bars are smaller than the

symbols representing the data points. Right - decolorization of crystal violet. From left to right:

A - dye + H_2O; B - dye + H_2O_2; C - dye + H_2O + ferrous sulfate (10 %) modified textile treated

by microwave irradiation; D - dye + H_2O_2 + ferrous sulfate (10 %) modified textile treated by

microwave irradiation. Reaction time was 10 min at room temperature.

4.   Conclusions

In summary, extremely simple, green and low-cost procedures for the preparation of textile bound magnetic iron oxide particles exhibiting peroxidase-like activity were developed. Only one iron oxide precursor (ferrous sulfate) and cheap domestic microwave oven were employed in the course microwave-assisted textile modification.   Textile immobilized nanozyme was characterized in detail; the micro- and nanostructure as revealed by SEM and small-angle scattering shows specific surface morphologies based on the nanoparticle system used; MW-treated samples exhibit rough layers of larger particles and aggregates, while for textiles with ferrofluid MNPs, thinner and more homogenous films are adsorbed on the cotton fibers. The assembly of different NP aggregates on the cotton matrix leads to the formation of layers with different effective surface areas. Such a larger surface area for the MW-treated samples could then explain the stronger catalytic (peroxidase-like) activity observed than for the FF-based samples. The peroxidase-like activity enabled rapid decolorization of crystal violet in the presence of hydrogen peroxide; under experimental conditions used 10-15 min reaction time was sufficient. The simplicity of immobilized nanozyme preparation and low cost of all the precursors can enable its widespread application in order to substitute more expensive and sensitive free and immobilized peroxidases. Other types of woven and nonwoven textile materials with bound nanozymes can be prepared and used as low-cost catalysts for a variety of applications. Textile carrier modified with a piece of magnetic iron wire enables rapid separation of immobilized catalyst from large volumes of the reaction mixture.

Associated content

Supporting information

The Supporting Information is available free of charge at https://

Magnetization curves of water-based magnetic fluid (Figure S1); EDS of native cotton textile, cotton textile modified by microwave irradiation and cotton textile modified with acid ferrofluid (Figure S2); comparison of SAXS and SANS data (Figure S3); SAXS data for nanoparticles in suspension (Figure S4).

Notes

The authors declare no competing financial interest.

Main corresponding author

Ivo Safarik, Department of Nanobiotechnology, Biology Centre, ISB, CAS, Na Sadkach 7, 370 05 Ceske Budejovice, Czech Republic. Email: ivosaf@yahoo.com

Other corresponding authors

Martin A. Schroer, European Molecular Biology Laboratory (EMBL), Hamburg outstation c/o DESY, Notkestr. 85, 22607, Hamburg, Germany. Present address: Nanoparticle Process Technology, University of Duisburg-Essen, Lotharstr. 1, 47057 Duisburg, Germany. Email: martin.schroer@uni-due.de

Peter Kopcansky, Department of Magnetism, Institute of Experimental Physics, SAS, Watsonova 47, 040 01 Kosice, Slovakia. Email: kopcan@saske.sk

Viktor I. Petrenko, BCMaterials, Basque Center for Materials, Applications and Nanostructures, Leioa, Spain. Email: viktor.petrenko@bcmaterials.net

Author Contributions

The manuscript was written through contributions of all authors. All authors have given approval to the final version of the manuscript.

List of abbreviations

CV   crystal violet

DPD   N,N-diethyl-p-phenylenediamine sulfate salt

EDS   energy dispersive X-ray spectra

FF   ferrofluid

HRP   horseradish peroxidase

IONs   iron oxide nanozymes

MF   magnetic fluid

MNPs   magnetic nanoparticles

MW   microwave

NPs   nanoparticles

P-L   peroxidase-like

SANS   small-angle neutron scattering

SAS   small-angle scattering

SAXS   small-angle X-ray scattering

SEM   scanning electron microscopy

References

(1) Anastasova, E. I.; Prilepskii, A. Y.; Fakhardo, A. F.; Drozdov, A. S.; Vinogradov, V. V. Magnetite Nanocontainers: Toward Injectable Highly Magnetic Materials for Targeted Drug Delivery. *ACS Appl. Mater. Interfaces* **2018,** *10* (36), 30040-30044.

(2) Xu, J.; Zhu, K.; Hou, Y. Magnetic Heterostructures: Interface Control to Optimize Magnetic Property and Multifunctionality. *ACS Appl. Mater. Interfaces* **2020,** *12* (33), 36811-36822.

(3) Safarik, I.; Pospiskova, K.; Horska, K.; Safarikova, M. Potential of Magnetically Responsive (Nano)Biocomposites. *Soft Matter* **2012,** *8* (20), 5407-5413.

(4) Das, P.; Colombo, M.; Prosperi, D. Recent Advances in Magnetic Fluid Hyperthermia for Cancer Therapy. *Colloids Surf. B* **2019,** *174*, 42-55.

(5) Wang, Y.; Xu, C.; Chang, Y.; Zhao, L.; Zhang, K.; Zhao, Y.; Gao, F.; Gao, X. Ultrasmall Superparamagnetic Iron Oxide Nanoparticle for T2-Weighted Magnetic Resonance Imaging. *ACS Appl. Mater. Interfaces* **2017,** *9* (34), 28959-28966.

(6) Bulte, J. W. M. Superparamagnetic Iron Oxides as MPI Tracers: A Primer and Review of Early Applications. *Adv. Drug Deliv. Rev.* **2019,** *138*, 293-301.

(7) Bossis, G.; Lacis, S.; Meunier, A.; Volkova, O. Magnetorheological Fluids. *J. Magn. Magn. Mater.* **2002,** *252* (1-3), 224-228.

(8) Gao, L.; Zhuang, J.; Nie, L.; Zhang, J.; Zhang, Y.; Gu, N.; Wang, T.; Feng, J.; Yang, D.; Perrett, S.; Yan, X. Intrinsic Peroxidase-Like Activity of Ferromagnetic Nanoparticles. *Nat. Nanotechnol.* **2007,** *2* (9), 577-583.

(9) Gao, L. Z.; Fan, K. L.; Yan, X. Y. Iron Oxide Nanozyme: A Multifunctional Enzyme Mimetic for Biomedical Applications. *Theranostics* **2017,** *7* (13), 3207-3227.

(10) Wei, H.; Wang, E. Fe_3O_4 Magnetic Nanoparticles as Peroxidase Mimetics and Their Applications in H_2O_2 and Glucose Detection. *Anal. Chem.* **2008,** *80* (6), 2250-2254.

(11) Kim, M. I.; Shim, J.; Li, T.; Lee, J.; Park, H. G. Fabrication of Nanoporous Nanocomposites Entrapping Fe_3O_4 Magnetic Nanoparticles and Oxidases for Colorimetric Biosensing. *Chem. Eur. J.* **2011,** *17* (38), 10700-10707.

(12) Kim, M. I.; Shim, J.; Li, T.; Woo, M.-A.; Cho, D.; Lee, J.; Park, H. G. Colorimetric Quantification of Galactose Using a Nanostructured Multi-Catalyst System Entrapping Galactose Oxidase and Magnetic Nanoparticles as Peroxidase Mimetics. *Analyst* **2012,** *137* (5), 1137-1143.

(13) Il Kim, M.; Shim, J.; Parab, H. J.; Shin, S. C.; Lee, J.; Park, H. G. A Convenient Alcohol Sensor Using One-Pot Nanocomposite Entrapping Alcohol Oxidase and Magnetic Nanoparticles as Peroxidase Mimetics. *J. Nanosci. Nanotechnol.* **2012,** *12* (7), 5914-5919.

(14) Melnikova, L.; Pospiskova, K.; Mitroova, Z.; Kopcansky, P.; Safarik, I. Peroxidase-Like Activity of Magnetoferritin. *Microchim. Acta* **2014,** *181* (3-4), 295-301.

(15) Bilal, M.; Zhao, Y.; Rasheed, T.; Iqbal, H. M. N. Magnetic Nanoparticles as Versatile Carriers for Enzymes Immobilization: A Review. *Int. J. Biol. Macromol.* **2018,** *120*, 2530-2544.

(16) Zdarta, J.; Meyer, A. S.; Jesionowski, T.; Pinelo, M. A General Overview of Support Materials for Enzyme Immobilization: Characteristics, Properties, Practical Utility. *Catalysts* **2018,** *8* (2), 92.

(17) Basso, A.; Serban, S. Industrial Applications of Immobilized Enzymes - A Review. *Mol. Catal.* **2019,** *479*, 35-54.

(18) Opwis, K.; Straube, T.; Kiehl, K.; Gutmann, J. S. Various Strategies for the Immobilization of Biocatalysts on Textile Carrier Materials. *Chem. Eng. Trans.* **2014,** *38*, 223-228.

(19) Safarik, I.; Baldikova, E.; Safarikova, M.; Pospiskova, K. Magnetically Responsive Textile for a New Preconcentration Procedure: Magnetic Textile Solid Phase Extraction. *J. Ind. Text.* **2018,** *48* (4), 761-771.

(20) Safarik, I.; Mullerova, S.; Pospiskova, K. Semiquantitative Determination of Food Acid Dyes by Magnetic Textile Solid Phase Extraction Followed by Image Analysis. *Food Chem.* **2019,** *274*, 215-219.

(21) Safarik, I.; Prochazkova, J.; Baldikova, E.; Pospiskova, K. Textile Bound Methyltrioctylammonium Thiosalicylate Ionic Liquid for Magnetic Textile Solid Phase Extraction of Copper Ions. *J. Mol. Liq.* **2019,** *296,* 111910.

(22) Kiehl, K.; Straube, T.; Opwis, K.; Gutmann, J. S. Strategies for Permanent Immobilization of Enzymes on Textile Carriers. *Eng. Life Sci.* **2015,** *15* (6), 622-626.

(23) Feng, J.; Hontañón, E.; Blanes, M.; Meyer, J.; Guo, X.; Santos, L.; Paltrinieri, L.; Ramlawi, N.; Smet, L. C. P. M. d.; Nirschl, H.; Kruis, F. E.; Schmidt-Ott, A.; Biskos, G. Scalable and Environmentally Benign Process for Smart Textile Nanofinishing. *ACS Appl. Mater. Interfaces* **2016,** *8* (23), 14756-14765.

(24) Prochazkova, J.; Pospiskova, K.; Safarik, I. Magnetically Modified Electrospun Nanotextile Exhibiting Peroxidase-Like Activity. *J. Magn. Magn. Mater.* **2019,** *473*, 335-340.

(25) Yetisen, A. K.; Qu, H.; Manbachi, A.; Butt, H.; Dokmeci, M. R.; Hinestroza, J. P.; Skorobogatiy, M.; Khademhosseini, A.; Yun, S. H. Nanotechnology in Textiles. *ACS Nano* **2016,** *10* (3), 3042-3068.

(26) Baldikova, E.; Pospiskova, K.; Safarikova, M.; Safarik, I. Non-Woven Fabric Supported Manganese Dioxide Microparticles as a Low-Cost, Easily Recoverable Catalyst for Hydrogen Peroxide Decomposition. *Mater. Chem. Phys.* **2018,** *203*, 280-283.

(27) Harifi, T.; Montazer, M. In Situ Synthesis of Iron Oxide Nanoparticles on Polyester Fabric Utilizing Color, Magnetic, Antibacterial and Sono-Fenton Catalytic Properties. *J. Mater, Chem. B* **2014,** *2* (3), 272-282.

(28) Bunoiu, M.; Anitas, E. M.; Pascu, G.; Chirigiu, L. M. E.; Bica, I. Electrical and Magnetodielectric Properties of Magneto-Active Fabrics for Electromagnetic Shielding and Health Monitoring. *Int. J. Mol. Sci.* **2020,** *21* (13), 4785.

(29) Coulibaly, G. N.; Rtimi, S.; Assadi, A. A.; Hanna, K. Nano-Sized Iron Oxides Supported on Polyester Textile to Remove Fluoroquinolones in Hospital Wastewater. *Environ. Sci. Nano* **2020,** *7* (7), 2156-2165.

(30) Harifi, T.; Montazer, M. Photo-, Bio-, and Magneto-active Colored Polyester Fabric with Hydrophobic/Hydrophilic and Enhanced Mechanical Properties through Synthesis of $TiO_2/Fe_3O_4/Ag$ Nanocomposite. *Ind. Eng. Chem. Res.* **2014,** *53* (3), 1119-1129.

(31) Safarik, I.; Pospiskova, K.; Baldikova, E.; Savva, I.; Vekas, L.; Marinica, O.; Tanasa, E.; Krasia-Christoforou, T. Fabrication and Bioapplications of Magnetically Modified Chitosan-Based Electrospun Nanofibers. *Electrospinning* **2018,** *2* (1), 29-39.

(32) Ding, X. J.; Yu, M.; Wang, Z. Q.; Zhang, B. W.; Li, L. F.; Li, J. Y. A Promising Clean Way to Textile Colouration: Cotton Fabric Covalently-Bonded with Carbon Black, Cobalt Blue, Cobalt Green, and Iron Oxide Red Nanoparticles. *Green Chem.* **2019,** *21* (24), 6611-6621.

(33) Rastgoo, M.; Montazer, M.; Malek, R. M. A.; Harifi, T.; Rad, M. M. Ultrasound Mediation for One-Pot Sonosynthesis and Deposition of Magnetite Nanoparticles on Cotton/Polyester Fabric as a Novel Magnetic, Photocatalytic, Sonocatalytic, Antibacterial and Antifungal Textile. *Ultrason. Sonochem.* **2016,** *31*, 257-266.

(34) Montazer, M.; Harifi, T. Magnetic Nanofinishes for Textiles. In *Nanofinishing of Textile Materials*; Montazer, M.; Harifi, T., Eds.; Woodhead Publishing: 2018; pp 225-240.

(35) Safarik, I.; Safarikova, M. One-step Magnetic Modification of Non-Magnetic Solid Materials. *Int. J. Mater. Res.* **2014,** *105* (1), 104-107.

(36) Massart, R. Preparation of Aqueous Magnetic Liquids in Alkaline and Acidic Media. *IEEE Trans. Magn.* **1981,** *17* (2), 1247-1248.

(37) Baldikova, E.; Politi, D.; Maderova, Z.; Pospiskova, K.; Sidiras, D.; Safarikova, M.; Safarik, I. Utilization of Magnetically Responsive Cereal By-Product for Organic Dye Removal. *J. Sci. Food Agr.* **2016,** *96* (6), 2204-2214.

(38) Bader, H.; Sturzenegger, V.; Hoigné, J. Photometric Method for the Determination of Low Concentrations of Hydrogen Peroxide by the Peroxidase Catalyzed Oxidation of N,N-diethyl-p-phenylenediamine (DPD). *Water Res.* **1988,** *22* (9), 1109-1115.

(39) Blanchet, C. E.; Spilotros, A.; Schwemmer, F.; Graewert, M. A.; Kikhney, A.; Jeffries, C. M.; Franke, D.; Mark, D.; Zengerle, R.; Cipriani, F.; Fiedler, S.; Roessle, M.; Svergun, D. I. Versatile Sample Environments and Automation for Biological Solution X-Ray Scattering Experiments at the P12 Beamline (PETRA III, DESY). *J. Appl. Crystallogr.* **2015,** *48*, 431-443.
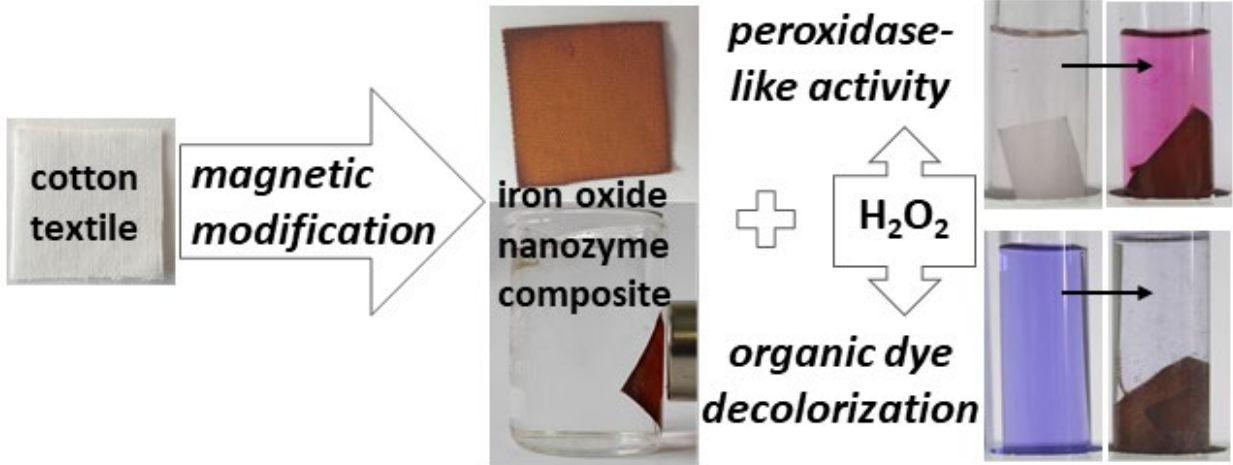
(40) Kraft, P.; Bergamaschi, A.; Broennimann, C.; Dinapoli, R.; Eikenberry, E. F.; Henrich, B.; Johnson, I.; Mozzanica, A.; Schleputz, C. M.; Willmott, P. R.; Schmitt, B. Performance of Single-Photon-Counting PILATUS Detector Modules. *J. Synchrotron Radiat.* **2009,** *16*, 368-375.

(41) Franke, D.; Kikhney, A. G.; Svergun, D. I. Automated Acquisition and Analysis of Small Angle X-Ray Scattering Data. *Nucl. Instrum. Meth. A* **2012,** *689*, 52-59.

(42) Franke, D.; Petoukhov, M. V.; Konarev, P. V.; Panjkovich, A.; Tuukkanen, A.; Mertens, H. D. T.; Kikhney, A. G.; Hajizadeh, N. R.; Franklin, J. M.; Jeffries, C. M.; Svergun, D. I. ATSAS 2.8: A Comprehensive Data Analysis Suite for Small-Angle Scattering from Macromolecular Solutions. *J. Appl. Crystallogr.* **2017,** *50*, 1212-1225.

(43) Svergun, D. I. Determination of the Regularization Parameter in Indirect-Transform Methods Using Perceptual Criteria. *J. Appl. Crystallogr.* **1992,** *25*, 495-503.

(44) Kuklin, A. I.; Ivankov, A. I.; Soloviov, D. V.; Rogachev, A. V.; Kovalev, Y. S.; Soloviev, A. G.; Islamov, A. K.; Balasoiu, M.; Vlasov, A. V.; Kutuzov, S. A.; Sirotin, A. P.; Kirilov, A. S.; Skoi, V. V.; Rulev, M. I.; Gordeliy, V. I. High-Throughput SANS Experiment on Two-Detector System of YuMO Spectrometer. *J. Phys. Conf. Ser.* **2018,** *994*, 012016.

(45) Soloviev, A. G.; Solovjeva, T. M.; Ivankov, O. I.; Soloviov, D. V.; Rogachev, A. V.; Kuklin, A. I. SAS Program for Two-Detector system: Seamless Curve from Both Detectors. *J. Phys. Conf. Ser.* **2017,** *848*, 012020.

(46) Glatter, O. New Method for Evaluation of Small-Angle Scattering Data. *J. Appl. Crystallogr.* **1977,** *10*, 415-421.

(47) Pedersen, J. S. Analysis of Small-Angle Scattering Data from Colloids and Polymer Solutions: Modeling and Least-Squares Fitting. *Adv. Colloid Interface Sci.* **1997,** *70*, 171-210.

(48) Safarik, I.; Baldikova, E.; Prochazkova, J.; Safarikova, M.; Pospiskova, K. Magnetically Modified Agricultural and Food Waste: Preparation and Application. *J. Agr. Food Chem.* **2018,** *66* (11), 2538-2552.

(49) Safarik, I.; Horska, K.; Pospiskova, K.; Maderova, Z.; Safarikova, M. Microwave Assisted Synthesis of Magnetically Responsive Composite Materials. *IEEE Trans. Magn.* **2013,** *49* (1), 213-218.

(50) Safarik, I.; Prochazkova, J.; Baldikova, E.; Timko, M.; Kopcansky, P.; Rajnak, M.; Torma, N.; Pospiskova, K. Modification of Diamagnetic Materials Using Magnetic Fluids. *Ukr. J. Phys.* **2020,** *65* (9), 751-760.

(51) Rabbi, M. A.; Rahman, M. M.; Minami, H.; Yamashita, N.; Habib, M. R.; Ahmad, H. Magnetically Responsive Antibacterial Nanocrystalline Jute Cellulose Nanocomposites with Moderate Catalytic Activity. *Carbohydr. Polym.* **2021,** *251*, 117024.

(52) Perelshtein, I.; Applerot, G.; Perkas, N.; Guibert, G.; Mikhailov, S.; Gedanken, A. Sonochemical Coating of Silver Nanoparticles on Textile Fabrics (Nylon, Polyester and Cotton) and their Antibacterial Activity. *Nanotechnology* **2008,** *19* (24), 245705.

(53) Perera, S.; Bhushan, B.; Bandara, R.; Rajapakse, G.; Rajapakse, S.; Bandara, C. Morphological, Antimicrobial, Durability, and Physical Properties of Untreated and Treated Textiles Using Silver-Nanoparticles. *Colloids Surf. A* **2013,** *436*, 975-989.

(54) Marsh, D. H.; Riley, D. J.; York, D.; Graydon, A. Sorption of Inorganic Nanoparticles in Woven Cellulose Fabrics. *Particuology* **2009,** *7* (2), 121-128.

(55) Raşa, M.; Bica, D.; Philipse, A.; Vékás, L. Dilution Series Approach for Investigation of Microstructural Properties and Particle Interactions in High-Quality Magnetic Fluids. *Eur. Phys. J. E* **2002,** *7*, 209–220.

(56) Goya, G. F.; Berquó, T. S.; Fonseca, F. C. Static and Dynamic Magnetic Properties of Spherical Magnetite Nanoparticles. *J. Appl. Phys*. **2003,** *94*, 3520.

(57) Rosensweig, R. E. *Ferrohydrodynamics*, Dover Publications: 2013.

(58) Martinez-Sanz, M.; Pettolino, F.; Flanagan, B.; Gidley, M. J.; Gilbert, E. P. Structure of Cellulose Microfibrils in Mature Cotton Fibres. *Carbohydr. Polym.* **2017,** *175*, 450-463.

(59) Gdovinova, V.; Schroer, M. A.; Tomasovicova, N.; Appel, I.; Behrens, S.; Majorosova, J.; Kovac, J.; Svergun, D. I.; Kopcansky, P. Structuralization of Magnetic Nanoparticles in 5CB Liquid Crystals. *Soft Matter* **2017,** *13* (43), 7890-7896.

(60) Beaucage, G. Small-Angle Scattering from Polymeric Mass Fractals of Arbitrary Mass-Fractal Dimension. *J. Appl. Crystallogr.* **1996,** *29* (2), 134-146.

(61) Chang, Q.; Deng, K.; Zhu, L.; Jiang, G.; Yu, C.; Tang, H. Determination of Hydrogen Peroxide with the Aid of Peroxidase-Like Fe_3O_4 Magnetic Nanoparticles as the Catalyst. *Microchim. Acta* **2009,** *165* (3), 299.

(62) Husain, Q. Peroxidase Mediated Decolorization and Remediation of Wastewater Containing Industrial Dyes: A Review. *Rev. Environ. Sci. Biotechnol.* **2010,** *9* (2), 117-140.

(63) Singh, R. L.; Singh, P. K.; Singh, R. P. Enzymatic Decolorization and Degradation of Azo Dyes – A Review. *Int. Biodeterior. Biodegradation* **2015,** *104*, 21-31.

(64) Bhunia, A.; Durani, S.; Wangikar, P. P. Horseradish Peroxidase Catalyzed Degradation of Industrially Important Dyes. *Biotechnol. Bioeng.* **2001,** *72* (5), 562-567.

(65) Liu, J.-Z.; Wang, T.-L.; Ji, L.-N. Enhanced Dye Decolorization Efficiency by Citraconic Anhydride-Modified Horseradish Peroxidase. *J. Mol. Catal. B Enzym.* **2006,** *41* (3), 81-86.

(66) Ulson de Souza, S. M. A. G.; Forgiarini, E.; Ulson de Souza, A. A. Toxicity of Textile Dyes and Their Degradation by the Enzyme Horseradish Peroxidase (HRP). *J. Hazard. Mater.* **2007,** *147* (3), 1073-1078.

(67) Nasab, S. G.; Semnani, A.; Teimouri, A.; Yazd, M. J.; Isfahani, T. M.; Habibollahi, S. Decolorization of Crystal Violet from Aqueous Solutions by a Novel Adsorbent Chitosan/Nanodiopside Using Response Surface Methodology and Artificial Neural Network-Genetic Algorithm. *Int. J. Biol. Macromol.* **2019,** *124*, 429-443.

(68) Sadaf, A.; Ahmad, R.; Ghorbal, A.; Elfalleh, W.; Khare, S. K. Synthesis of Cost-Effective Magnetic Nano-Biocomposites Mimicking Peroxidase Activity for Remediation of Dyes. *Environ. Sci. Pollut. Res.* **2020,** *27* (22), 27211-27220.

Cotton textile/iron oxide nanozyme composites with peroxidase-like activity: Preparation, characterization and application

Ivo Safarik[1,2,3,*], Jitka Prochazkova[1], Martin A. Schroer[4,*], Vasil M. Garamus[5], Peter Kopcansky[3,*], Milan Timko[3], Michal Rajnak[3,6], Maksym Karpets[3,6], Oleksandr I. Ivankov[7], Mikhail V. Avdeev[7], Viktor I. Petrenko[8,9,*], Leonid Bulavin[10], Kristyna Pospiskova[1,2]

[1] Department of Nanobiotechnology, Biology Centre, ISB, CAS, Na Sadkach 7, 370 05 Ceske Budejovice, Czech Republic

[2] Regional Centre of Advanced Technologies and Materials, Palacky University, Slechtitelu 27, 783 71 Olomouc, Czech Republic

[3] Department of Magnetism, Institute of Experimental Physics, SAS, Watsonova 47, 040 01 Kosice, Slovakia

[4] European Molecular Biology Laboratory (EMBL), Hamburg outstation c/o DESY, Notkestr. 85, 22607, Hamburg, Germany. Present address: Nanoparticle Process Technology, University of Duisburg-Essen, Lotharstr. 1, 47057, Duisburg, Germany.

[5] Helmholtz-Zentrum Hereon, Max-Planck-Str. 1, Geesthacht 21502, Germany

[6] Faculty of Electrical Engineering and Informatics, Technical University of Košice, Letná 9, 04200 Košice, Slovakia

[7] Joint Institute for Nuclear Research, Dubna, Moscow region, Russia

[8] BCMaterials, Basque Center for Materials, Applications and Nanostructures, Leioa, Spain

[9] IKERBASQUE, Basque Foundation for Science, Bilbao, Spain

[10] Taras Shevchenko National University of Kyiv, 64/13, Volodymyrs'ka Str., Kyiv 01601, Ukraine
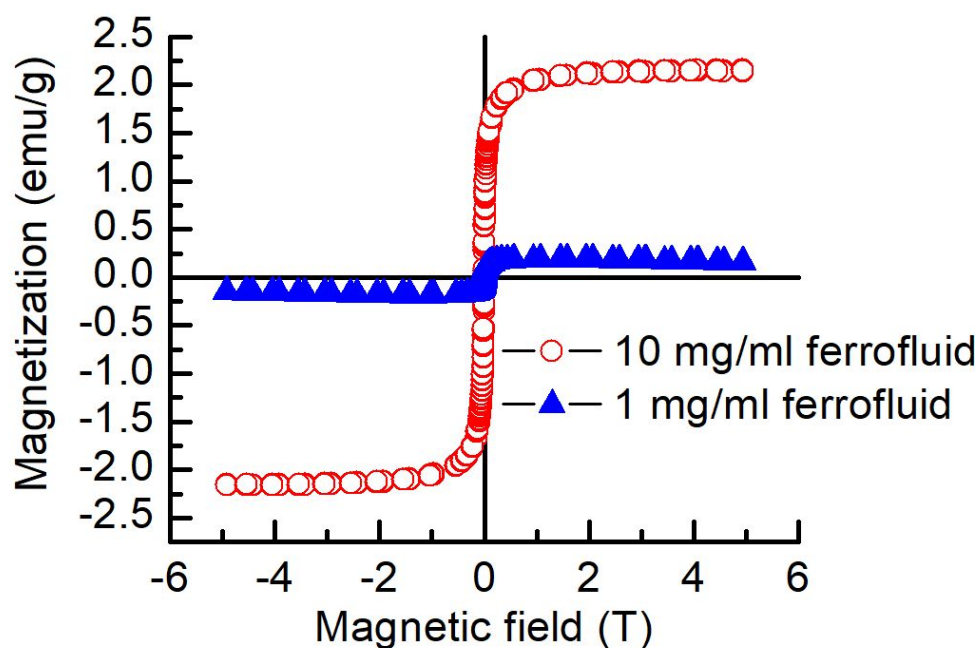
Figure S1. Magnetization curves of water-based magnetic fluid stabilized with perchloric acid at two concentrations (10 mg mL^{-1} and 1 mg mL^{-1}, respectively).

The ferrofluid magnetization was measured on a sample of 30 μL hermetically sealed in a specialized capsule. The diamagnetic signal from the capsule has been subtracted from the total magnetization. The slight decrease in magnetization measured on FF 1 mg mL^{-1} at higher magnetic fields is ascribed to the diamagnetic contribution of water, which is not negligible due to the low nanoparticle concentration. From the curves, the following magnetizations of saturation are found for FF 1 mg mL^{-1} (0.19 emu g^{-1}) and FF 10 mg mL^{-1} (2.15 emu g^{-1}), respectively.
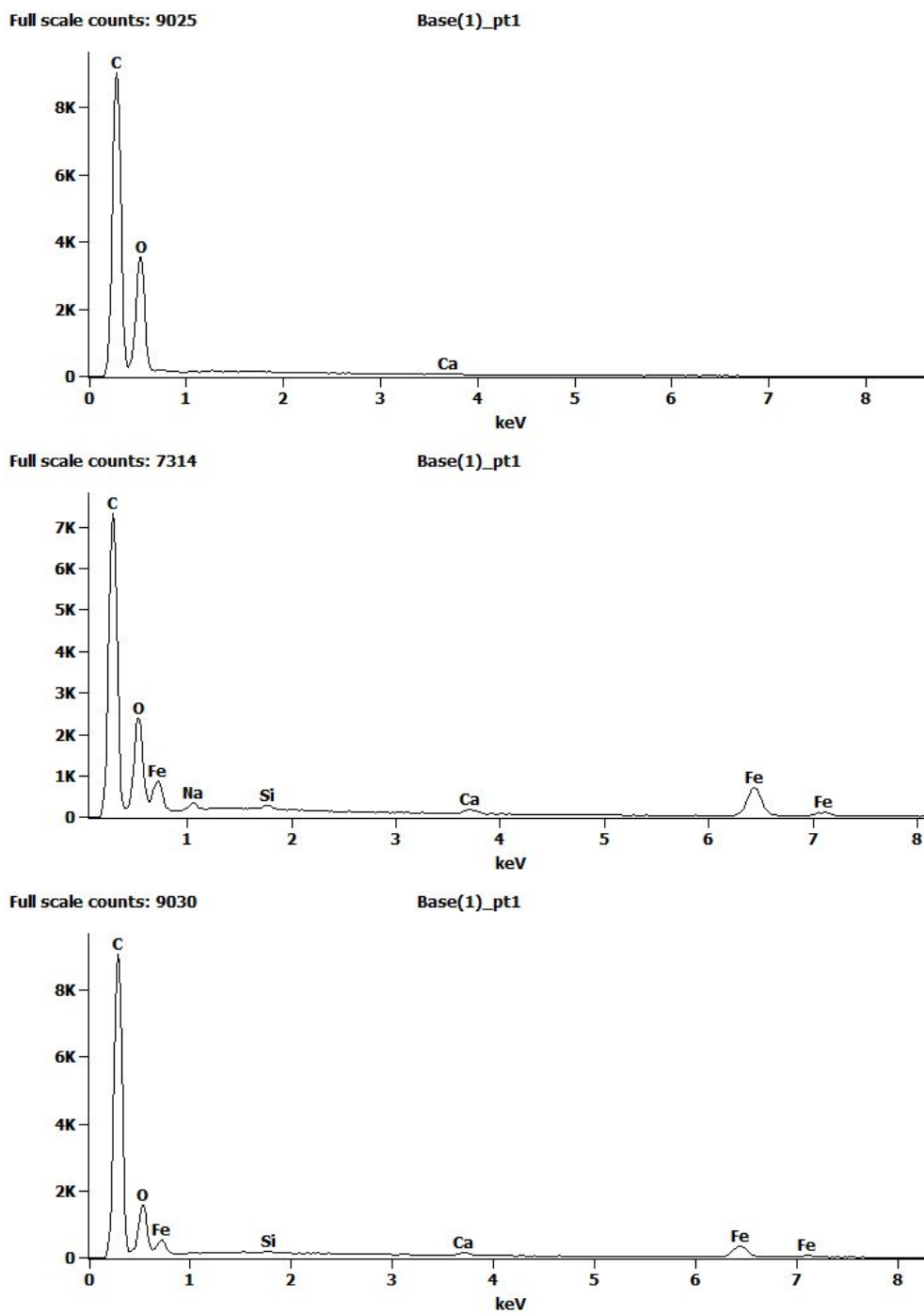
Figure S2. EDS (from top to bottom) of native cotton textile, cotton textile modified by microwave irradiation (20 % $FeSO_4 . 7H_2O$ solution used) and cotton textile modified with acid ferrofluid (concentration 10 mg mL^{-1} used).
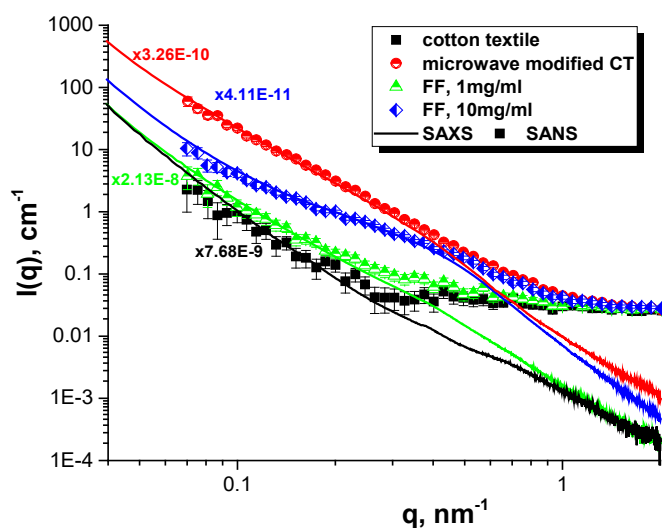
Figure S3. Comparison of SAXS and SANS data after corresponding multiplication on various scale factors.

In order to compare how the structure of the adsorbed nanoparticles differs from the one in suspension, SAXS data were collected from the two nanoparticle suspensions (ferrofluid and nanoparticles prepared by the microwave-assisted synthesis [1-2]) and are shown in Figure S4. Both nanoparticles in suspension can be described as a composition of two particle species: Small particles and large aggregates formed from the smaller ones. As is reflected from the pair distance distribution function p(r), the small particles for both samples exhibit roughly spherical shape, with the ones used from the MW-assisted synthesis having an average particle radius $R = 2.8$ nm and the ferrofluid of $R = 5.9$ nm. It has to be noted though, that the presence of shape and size dispersity, as also shown by the SEM images, limits a more detailed analysis. The aggregates formed by the ferrofluid exhibit on average an elongated form with maximum size $d_{max} = 170$ nm and an apparent short axis of ca. 40 nm (position of the maximum), while the other nanoparticle form diffuse aggregates of less obvious shape. The formation of elongated aggregates for ferrofluids has been observed previously [3].
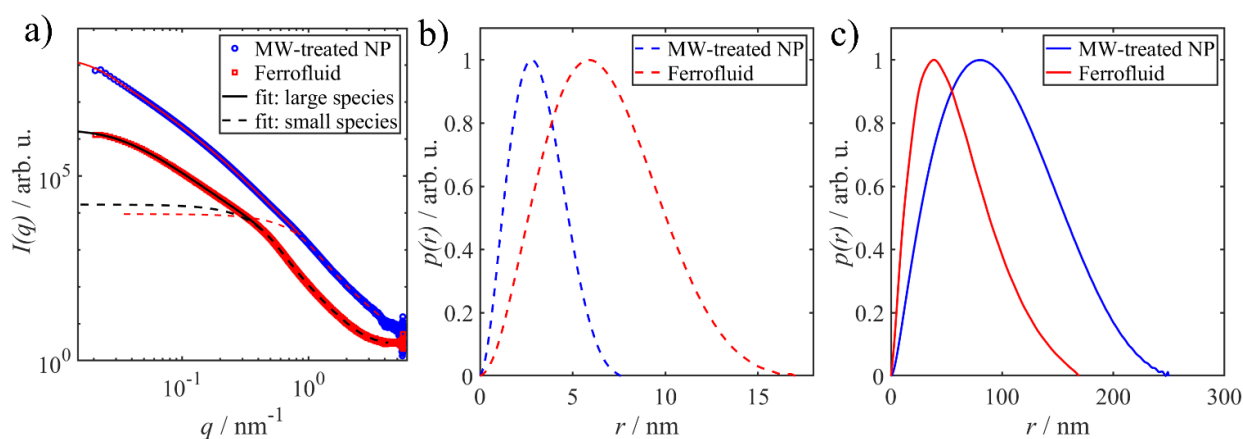
Figure S4. SAXS data for nanoparticles in suspension. a) SAXS curves for nanoparticles used for the microwave-assisted synthesis (MW-treated NP) and of the ferrofluid. Solid lines: GNOM fits for the large particle species, dashed lines: GNOM fits for the small species. Corresponding pair distance distribution function p(*r*); b) for the smaller particle species and c) for the larger aggregates.

References

(1) Safarik, I.; Safarikova, M. One-Step Magnetic Modification of Non-Magnetic Solid Materials. *Int. J. Mater. Res.* **2014,** *105* (1), 104-107.

(2) Baldikova, E.; Politi, D.; Maderova, Z.; Pospiskova, K.; Sidiras, D.; Safarikova, M.; Safarik, I. Utilization of Magnetically Responsive Cereal By-Product for Organic Dye Removal. *J. Sci. Food Agr.* **2016,** *96* (6), 2204-2214.

(3) Gdovinova, V.; Schroer, M. A.; Tomasovicova, N.; Appel, I.; Behrens, S.; Majorosova, J.; Kovac, J.; Svergun, D. I.; Kopcansky, P. Structuralization of Magnetic Nanoparticles in 5CB Liquid Crystals. *Soft Matter* **2017,** *13* (43), 7890-7896.